Minimal Model for Transport Barrier Dynamics Based on Ion-Temperature-Gradient Turbulence

G. Hu

Department of Physics, University of California, Irvine, CA 92717, USA

and

W. Horton

Institute for Fusion Studies, The University of Texas at Austin

Austin, Texas 78712 USA

August 28, 1997

Abstract

Low-order mode coupling equations are derived to describe recent computer simulations of the toroidal ion-temperature-gradient turbulent convection with steady and pulsating sheared mass flows in the transport barrier zone. The three convective transport states are identified with the tokamak confinement regimes called low mode (L-mode), high mode (H-mode), and barrier localized modes (BLMs) when the transport barrier is in the core plasma. The L-mode limit cycle is analytically derived and a bifurcation diagram showing L to H and H to BLM transitions in confinement is constructed numerically. Markovian closure procedures are sought to further reduce the dimensionality of the nonlinear system. First an exact expression is given for the energy transfer rate from the fluctuations to the sheared mass flow through the triplet velocity correlation function. Then the time scale expansion required to derive the Markovian closure formula is given. Markovian closure formulas form the basis for the thermodynamic-like L-H bifurcation models.

PACS nos.: 52.25.Fi, 52.35.Kt, 52.35.Ra, 52.55.Fa

I Introduction

An important method for understanding the nonlinear physics of hydrodynamic and plasma systems governed by partial differential equations is the projection of the dynamics onto a low-dimensional set of modes. Important examples are the Lorenz system [1] for Rayleigh-Benard convection, the Kells-Orszag system [2] for the Euler equation and the Terry-Horton system [3] for dissipative drift waves. Recently, laboratory experiments for Rayleigh-Benard convections at low Prandtl numbers and computer simulations have shown the onset of sheared mass flows corresponding to a second bifurcation in the Rayleigh-Benard system. Low-order truncations showing such a similar sequence of bifurcations were presented by Howard and Krishnamurti [4] for the Rayleigh-Benard system. The original 6 ordinary differential equation (6-ODE) system has been extended by Thiffeault-Horton [5] to improve its accuracy for the Rayleigh-Benard system. Since self-generated shear flows are also observed in computer simulations of plasmas and thought to be observed in the L-H-ELM sequence of plasmas confinement states, corresponding low-dimensional plasma systems have been derived for the resistive-g plasma model which closely parallels the Rayleigh-Benard system of equations. The drift wave problem, however, contains waves in the first bifurcation from the stable state and thus has intrinsically twice the number of degrees of freedom compared with the Rayleigh-Benard problem.

Here we present and analyze a new low-dimensional model for the ion-temperature-gradient (ITG) driven convection in axisymmetric toroidal geometry. The model contains eleven nonlinearly coupled ordinary differential equations (11-ODE model) to describe the sequence of bifurcations corresponding to the L-mode with oscillating drift waves, the H-mode with drift waves and sheared flows and BLM states that have recurrence oscillations between these two types of confinement states. The increased complexity of a $d = 11$ system over earlier models is required by the existence of drift waves in the system.

The organization of the work is as follows: In Sec. II we present the partial differential equation model of the ITG system and give the projection of the system onto the $d = 11$ state space. In the process the linear stability analysis is shown to lead to modification of the classical Rayleigh number Ra to $\mathrm{Ra}^{\mathrm{eff}}$ for the ITG system. In Sec. III the analytic solution for the L-mode attractor is found by introducing appropriate quadratic variables. The second and third bifurcations are given with numerical examples. The dissipationless limit is briefly discussed. In Sec. IV the reduced, Markovian thermodynamic model is derived by closing the triplet correlation functions in terms of the three basic energy components. Section V gives the conclusions and the outlook for applications.

II Low-Order Mode Coupling Equations

The toroidal ion-temperature-gradient dynamics in the Horton-Choi-Tang [6] (hereafter HCT) two-component fluid model is given by the following coupled vorticity and pressure equations:

$$\frac{d}{dt}\left(1-\nabla_\perp^2\right)\phi = -v_d\left[1-2\epsilon_n+K_i\nabla_\perp^2\right]\frac{\partial\phi}{\partial y}+2\epsilon_n\frac{\partial p}{\partial y}-\mu\nabla^4\phi \tag{1}$$

$$\frac{d}{dt}p = -v_d\overline{K}_i\frac{\partial\phi}{\partial y}+\kappa\nabla_\perp^2 p \tag{2}$$

where the d/dt is the two-dimensional (2D) convective derivative

$$\frac{df}{dt} = \frac{\partial f}{\partial t}+\frac{c}{B}[\phi,f] = \frac{\partial f}{\partial t}+\frac{c}{B}\left(\frac{\partial\phi}{\partial x}\frac{\partial f}{\partial y}-\frac{\partial\phi}{\partial y}\frac{\partial f}{\partial x}\right) \tag{3}$$

where the Poisson bracket $[\phi, f]$ arises from the $\mathbf{E}\times\mathbf{B}$ flow $\mathbf{v} = -c\nabla\phi\times\hat{\mathbf{z}}/B$. Here $K_i = \frac{T_i}{T_e}(\eta_i+1)$ and $\overline{K}_i = \frac{T_i}{T_e}(\eta_i+1-\Gamma_{\mathrm{eff}})$ are dimensionless measures of the ion pressure gradient. The parameter $\eta_i = (\partial_x \ln T_i)/(\partial_x \ln n) = L_n/L_{Ti}$ measures the strength of the ion temperature gradient relative to the density gradient. The parameter Γ_{eff} is the effective adiabatic gas constant that controls the onset of energy release from the interchange of flux tubes. The dimensionless measure of the toroidal curvature is given by $\epsilon_n = L_n/R$.

The $\mathbf{E}\times\mathbf{B}$ flow in the toroidal magnetic field $B = R_0B_0/(R_0 + r\cos\theta)$ has compression measured by $2\epsilon_n\partial_y\phi$, giving the downshift in the drift wave speed in Eq. (1). The diamagnetic currents $\mathbf{j}_{\rm dia} = \mathbf{B}\times\nabla p/B^2$ produce charge separation given by $2\epsilon_n\partial p/\partial y$ in the vorticity equation (1). In the original HCT model the compressional term $2\Gamma_{\rm eff}\partial\phi/\partial y$ in the pressure equation (2) was dropped. In Hong-Horton [7] the compression terms and the effective value of the adiabatic gas constant $\Gamma_{\rm eff}$ are shown to yield the correct threshold $\eta_{i,\rm crit}$ ($\simeq \Gamma_{\rm eff} - 1$) for the fluid description. Here we concentrate on states of turbulent convection well beyond the adiabatic threshold value, and thus follow HCT in neglecting the difference between K_i and $\overline{K}_i$. In the Appendix we discuss the kinetic form of the coefficients in Eqs. (1) and (2) obtained from the fluid limit of the Vlasov equation [8]. The role of the ion acoustic waves are treated in HCT but dropped in the present analysis for reasons discussed in the Appendix.

The vorticity equation follows from the quasineutrality condition $\nabla\cdot\mathbf{j} = 0$ with adiabatic electrons having the electron contribution $\nabla_\parallel j^e_\parallel = (n_e e^2/T_e)(\partial_t + v_d\partial_y)\phi$ where in the standard drift-wave units $x, y \to \rho_s x, \rho_s y$ and $t \to (L_n/c_s)t$ the drift speed $v_d = cT_e/eB\,L_n = c_s\rho_s/L_n = 1$. The collisional dissipation becomes $\mu = 0.3\nu_i\rho_i^2$ and $\kappa = 2.0\nu_i\rho_i^2$ becoming 0.3 and 2 times $(\nu_i L_n/c_s)(T_i/T_e)$ in the dimensionless units. The Prandtl number $\mathrm{Pr} = \mu/\kappa \approx 0.15$ in the system. The term $d\nabla_\perp^2\phi/dt$ is the nonlinear polarization drift as in the Hasegawa-Mima equation and the $K_i\nabla_\perp^2\partial_y\phi$ term is from the curl of the divergence of the ion current due to the finite-Larmor-radius (FLR) stress tensor ($\nabla\cdot\hat{\mathbf{z}}\times\nabla\cdot\boldsymbol{\pi}^{\rm FLR}$) and the cancelling part of the ion diamagnetic fluid velocity v_{di}. In the absence of the toroidal drift charge separation $2\epsilon_n\partial p/\partial y \to 0$, the FLR-drift-wave from Eq. (1) and (2) has the dispersion relation

$$\omega_{\mathbf{k}} = \frac{k_y v_d\,[1 - K_i k_\perp^2]}{1 + k_\perp^2} \tag{4}$$

where $\omega_{\mathbf{k}}$ is in units of c_s/L_n and k in units of ρ_s^{-1}. In Eq. (4), we also dropped the $2\epsilon_n$ term in the expression $[1 - 2\epsilon_n - K_i k_\perp^2]$ for simplicity while noting here that for applications

the $2\epsilon_n$ term tends to be important. The short wave components propagate in the ion diamagnetic direction and the long wave components in the electron diamagnetic direction. We will show that the intermediate waves where $k_\perp^2 \simeq K_i^{-1} = \frac{T_e}{T_i(1+\eta_i)} \ll 1$ give the largest anomalous thermal flux on the L-mode attractor. These modes are also close to maximizing the linear growth rate. These modes will be shown to have L-H-BLM properties similar to those reported in Horton-Hu-Laval [9] (hereafter HHL) for resistive g-modes. These fast-growing, slowly rotating fluctuations are also the first modes to resonate with the thermal ions since $k_\| v_i \ll |k_y v_d|$ and $\omega_{Di} \ll |k_y v_d|$ is assumed in the hydrodynamic expansion of the kinetic equations. The effect of the resonant ions is given in detail in Kim and Horton [10] and Kim, Kishimoto, Horton and Tajima [11]. The principal effect of the particle resonance is to determine the threshold $\eta_{i,\mathrm{crit}}$ for the instability. If we restrict consideration to states well above the marginal state, $K_i \gg K_{i,\mathrm{crit}}$, then $\gamma_k/\omega_k \gtrsim 0.05$ to 0.1 and the FLR–hydrodynamic description is valid. Gyrofluid effects can be incorporated into the present model by modifying the dissipative terms μ and κ as given in Waltz *et al.* [12] or Beer and Hammett [13]. For the $k_y = 0$ modes the appropriate form of the vorticity equation is modified by dropping the adiabatic response and using the neoclassical damping for the shear flows.

A. Linear stability analysis

For the HCT model the linear stability to fluctuations of the form $e^{i\mathbf{k}\cdot\mathbf{x}-i\omega t}$ is determined by the dispersion relation $D_\mathbf{k}(\omega) = 0$ where

$$D_\mathbf{k}(\omega) = \left[-i(1+k_\perp^2)\omega + ik_y u_k + \mu k_\perp^4\right](-i\omega + \kappa k^2) - k_y^2 I \tag{5}$$

where we define $u_k \equiv 1 - K_i k_\perp^2$, $g \equiv 2\epsilon_n$ and $I \equiv gK_i$.

From this equation one readily sees that the modes with vanishing drift-wave frequency $u_k = 0$ at $k_\perp^2 = 1/K_i$ have the same stability conditions as the resistive-g modes. Away from

these critical zero-frequency modes the phase rotates and the instability requires larger I. Taking ω real we find the marginal stability frequency for $\kappa \neq 0$ is given by

$$\omega_k = \frac{k_y u(k_\perp)}{1 + k^2 + (\mu/\kappa)k^2} \tag{6}$$

from $\mathrm{Im}(D_{\mathbf{k}}) = 0$. Thus, the Prandtl number $\mathrm{Pr} = \mu/\kappa$ controls the down shift of the marginal stability frequency from the FLR-drift-wave frequency $\omega_k^{dw} \equiv k_y u(k)/(1+k^2)$. We note that for $\mu = \kappa \equiv 0$, the dispersion relation is real for real ω and the marginal frequency is then $\frac{1}{2}\omega_k^{dw}$ and the stability condition following from the discriminant is $(\frac{1}{2}\omega_k^{dw})^2 \equiv k_y^2 I/(1+k^2)$. For real plasmas with either collisional or collisionless dissipation modelled by μ and κ, we have from Eq. (5) evaluated with Eq. (6) that

$$D_{\mathbf{k}}(\omega_k) = \frac{k_\perp^2 k_y^2 u^2(k_\perp)(\mu/\kappa)}{\left[1 + k_\perp^2(1+\mu/\kappa)\right]^2} + k_\perp^6 \mu\kappa - k_y^2 I. \tag{7}$$

The Nyquist diagram for Eq. (5) gives the condition for instability $D_{\mathbf{k}}(\omega_k) < 0$. The first

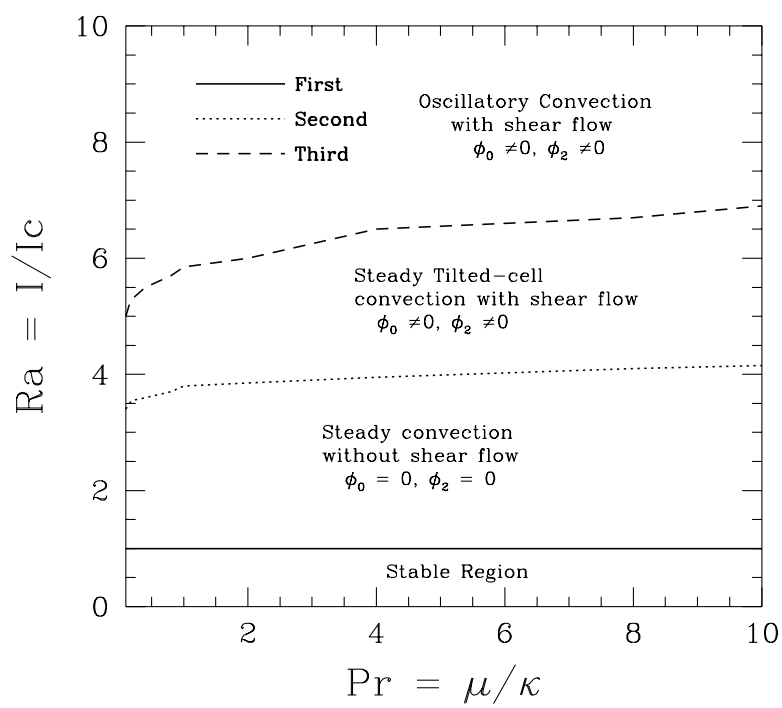

Figure 1: Bifurcation diagram showing the onset of convection numerically obtained in the parameter space of the Prandtl number and normalized Rayleigh number.

two terms in Eq. (7) are the stablizing terms while the third term is the driving term for the instability. In the absence of the drift-wave velocity, u_k, we see that the first mode to go unstable is $\min_{k_y}\left[(k_x^2+k_y^2)^3/k_y^2\right]$ at $k_y^2 = k_x^2/2$ giving the classical convection condition

$$I = gK_i > \frac{27}{4}\, k_x^4 \mu\kappa. \tag{8}$$

The classical value for free-slip follows from $k_x = \pi/L_x$ with $(27/4)\pi^4 \approx 658$. This leads to the definition of the Rayleigh number $\mathrm{Ra} = gK_iL_x^4/\mu\kappa$ and the well-known critical Rayleigh number $R_{\mathrm{crit}} = 658$.

For high temperature plasmas the drift-wave dispersion term dominates the $\mu\kappa$-dissipation in the most of the k-space. For $|k_y u_k| \gg k^2\kappa$ the first mode to go unstable minimizes the first term in Eq. (7) proportional to $u^2(k_\perp)$. This minimization occurs at $k_y^2 = 1/K_i \gg k_x^2$. There is no general agreement in the ITG-literature on the definition of the effective Rayleigh number. Here we give the following new definition in Eq. (9) based on the following observation. For the ITG instability Eq. (7) shows that there are two stabilizing effects. The first term in Eq. (7) is from the rotation of the wave phase due to the electron and ion diamagnetic drifts. The second stabilizing term is due to the dissipation as in the resistive-g and neutral fluid. As the temperature of the plasma increases the first term dominates the dissipation term and thus there is a change in the selection of the first mode number to go unstable and thus there is a change in the definition of the effective Rayleigh number from the classical value given in Eq. (8) to the value given in Eq. (9). When the diamagnetic drifts dominate the dissipation in Eq. (7), the first mode to go unstable is where the electron and ion diamagnetic drift effects cancel each other: $\omega_{\mathbf{k}} \approx k_y v_d\,[1 - 2\epsilon_n - K_i k_\perp^2] \approx 0$. Thus the selection of $k_\perp$ is determined by the parameter K_i and the ion gyroradius rather than the box size. The first mode to go unstable has the minimum value of k_x^2 which is always small compared with $k_y^2 = 1/K_i$. Therefore, the first mode to go unstable is $k_\perp^2 \approx k_y^2 = 1/K_i$ with minimum allowed k_x. In this k-region where the linear drift-wave frequency is reversing

direction, the $\mu\kappa$-dissipation stabilization again dominates. For these modes, the ratio of the driving-to-damping terms in Eq. (7) provide the definition

$$\mathrm{Ra}^{\mathrm{eff}} = \frac{I}{I_c} \approx \frac{I}{\mu\kappa k_\perp^4} = \frac{gK_i^3\rho_i^4}{\mu\kappa} \tag{9}$$

for the effective Rayleigh number. The measure given by Eq. (9) differs most notably from the classical Ra by its independence of the box size L_x and L_y.

The measure in Eq. (9) does have a strong dependence on the local density and temperature gradient scale lengths L_n, L_{T_i}. Using the collisional transport formulas for the viscosity and thermal diffusivity gives

$$\mathrm{Ra}^{\mathrm{eff}} = \frac{1.67 L_n^2 c_s^2}{\nu_i^2 L_{T_i}^3 R}$$

where c_s^2/R plays the role of gravity g in the torus. The lower bound on the ion collision frequency for the cross-field viscosity and thermal conductivity to apply is $\min(\nu_i) = v_i/qR$ so that $\mathrm{Ra}^{\mathrm{eff}}$ does not go to infinity in the collisionless limit due to dissipation from the wave-particle resonances. Using the limit $\min(\nu_i) = v_i/qR$ gives the $\max(\mathrm{Ra}^{\mathrm{eff}}) = (1.67T_e/T_i)(q^2RL_n^2/L_T^3)$. For tokamaks with steep temperature gradients this maximum $\mathrm{Ra}^{\mathrm{eff}}$ can readily reach 10^4. The key point is, however, that the effective Rayleigh number does not continue to increase with dimensions of the system as in classical systems. This is because the minimum $k_\perp$ is connected to the gyroradius rather than the system size.

B. 11-ODE mode coupling equations

Now we present the low-dimensional representation of the HCT equations (1) and (2). We adopt the Gelerkin approximation and choose the following low-order modes:

$$\begin{aligned}\phi = {} & \phi_0 \sin k_x x + \phi_1^s \sin k_x x \sin k_y y + \phi_1^c \sin k_x x \cos k_y y \\ & + \phi_2^s \sin 2k_x x \sin k_y y + \phi_2^c \sin 2k_x x \cos k_y y \end{aligned} \tag{10}$$

$$p = p_0 \sin k_x x + p_0' \sin 2k_x x + p_1^s \sin k_x x \sin k_y x + p_1^c \sin k_x x \cos k_y y$$

$$+ p_2^s \sin 2k_x x \sin k_y y + p_2^c \sin 2k_x x \cos k_y y. \tag{11}$$

Also let $k_0^2 = k_x^2, k_1^2 = k_x^2 + k_y^2, k_2^2 = 4k_x^2 + k_y^2, k_0'^2 = 4k_x^2, k_{xy}^2 = \frac{1}{2}k_x k_y$. The mode coupling equations can then be found:

$$\frac{\partial}{\partial t} k_0^2 \phi_0 = \frac{k_{xy}^2}{2}(k_1^2 - k_2^2)\left[\phi_1^s \phi_2^c - \phi_1^c \phi_2^s\right] - \mu^s k_0^4 \phi_0 \tag{12}$$

$$\frac{\partial}{\partial t}(k_1^2+1)\phi_1^s = k_{xy}^2\left(k_2^2 - k_0^2\right)\phi_0\phi_2^c + (1 - K_i k_1^2)k_y \phi_1^c - g k_y p_1^c - \mu k_1^4 \phi_1^s \tag{13}$$

$$\frac{\partial}{\partial t}(k_1^2+1)\phi_1^c = -k_{xy}^2\left(k_2^2 - k_0^2\right)\phi_0\phi_2^s - (1 - K_i k_1^2)k_y \phi_1^s + g k_y p_1^s - \mu k_1^4 \phi_1^c \tag{14}$$

$$\frac{\partial}{\partial t}(k_2^2+1)\phi_2^s = -k_{xy}^2\left(k_0^2 - k_1^2\right)\phi_0\phi_1^c + (1 - K_i k_2^2)k_y \phi_2^c - g k_y p_2^c - \mu k_2^4 \phi_2^s \tag{15}$$

$$\frac{\partial}{\partial t}(k_2^2+1)\phi_2^c = k_{xy}^2(k_0^2 - k_1^2)\phi_0\phi_1^s - (1 - K_i k_2^2)k_y \phi_2^s + g k_y p_2^s - \mu k_2^4 \phi_2^c; \tag{16}$$

and

$$\frac{\partial}{\partial t} p_0 = \frac{k_{xy}^2}{2}\left[p_1^s \phi_2^c - p_1^c \phi_2^s + p_2^s \phi_1^c - p_2^c \phi_1^s\right] - \kappa k_0^2 p_0 \tag{17}$$

$$\frac{\partial}{\partial t} p_0' = k_{xy}^2\left[p_1^c \phi_1^s - p_1^s \phi_1^c\right] - \kappa k_0^2 p_0' + P_{in} \tag{18}$$

$$\frac{\partial}{\partial t} p_1^s = k_{xy}^2\left[-p_0 \phi_2^c + p_2^c \phi_0 + 2p_0' \phi_1^c\right] + K_i k_y \phi_1^c - \kappa k_1^2 p_1^s \tag{19}$$

$$\frac{\partial}{\partial t} p_1^c = k_{xy}^2\left[p_0 \phi_2^s - p_2^s \phi_0 - 2p_0' \phi_1^s\right] - K_i k_y \phi_1^s - \kappa k_1^2 p_1^c \tag{20}$$

$$\frac{\partial}{\partial t} p_2^s = k_{xy}^2\left[-p_0 \phi_1^c + p_1^c \phi_0\right] + K_i k_y \phi_2^c - \kappa k_2^2 p_2^s \tag{21}$$

$$\frac{\partial}{\partial t} p_2^c = k_{xy}^2\left[p_0 \phi_1^s - p_1^s \phi_0\right] - K_i k_y \phi_2^s - \kappa k_2^2 p_2^c \tag{22}$$

where in Eq. (18) we have added the input heating power term P_{in}.

The quantity $k_{xy}^2 = k_x k_y/2$ arises from the $\mathbf{E} \times \mathbf{B}$ angular rotation frequency $\mathbf{k} \cdot \mathbf{v}_E \sim k_x k_y (c\phi_{\mathbf{k}}/B)$ measuring the strength of the mode coupling from a fluctuation of scale $\phi_{\mathbf{k}}$.

We choose parameters such that only the primary harmonic mode (ϕ_1^{sc}, p_1^{sc}) are linearly destabilized, while the secondary harmonic modes (ϕ_2^{sc}, p_2^{sc}) are linearly stable.

III Dynamical Bifurcations

A. Limit cycle on the L-mode attractor

The subset of modes $(\phi_1^s, \phi_1^c, p_1^s, p_1^c, p_0')$ forms a generalization of the three-dimensional (3D) Lorenz attractor from the first bifurcation which is the result of the linear instability. This is, for any set of initial values, the six other modes decay to zero so we have the $d_L = 5$ subdynamics

$$\frac{\partial}{\partial t}(1+k_1^2)\phi_1^s = (1-K_i k_1^2)k_y\phi_1^c - gk_y p_1^c - \mu k_1^4\phi_1^s \tag{23}$$

$$\frac{\partial}{\partial t}(1+k_1^2)\phi_1^c = -(1-K_i k_1^2)k_y\phi_1^s - gk_y p_1^s - \mu k_1^4\phi_1^c \tag{24}$$

$$\frac{\partial}{\partial t}p_0' = k_{xy}^2\left(p_1^c\phi_1^s - \phi_1^c p_1^s\right) - \chi^{\mathrm{nc}}k_0'^2 p_0' \tag{25}$$

$$\frac{\partial}{\partial t}p_1^s = 2k_{xy}^2 p_0'\phi_1^c + K_i k_y\phi_1^c - \kappa k_1^2 p_1^s \tag{26}$$

$$\frac{\partial}{\partial t}p_1^c = -2k_{xy}^2 p_0'\phi_1^s - K_i k_y\phi_1^s - \kappa k_1^2 p_1^c. \tag{27}$$

Due to the oscillatory characteristics of the waves, these modes will not reach a fixed point; rather they reach a limit cycle, as shown in Fig. 2. On the limit cycle the amplitudes $(|\phi_1^s|^2 + |\phi_1^c|^2)$ and $(|p_1^s|^2 + |p_1^c|^2)$ are constant. At this point it is convenient to define the following quadratic variables:

$$\Phi_1^2 = |\phi_1^s|^2 + |\phi_1^c|^2$$

$$P_1^2 = |p_1^s|^2 + |p_1^c|^2$$

$$\xi = p_1^s\phi_1^c - \phi_1^s p_1^c$$

$$\zeta = p_1^s\phi_1^s + \phi_1^c p_1^c.$$

Here Φ_1 and P_1 are the amplitude variables and ξ and ζ contain the relative phase of Φ_1 and

P_1.

From Eqs. (23) and (24) we have

$$\frac{1}{2}\frac{\partial}{\partial t}(1+k^2)\Phi_1^2 = gk_y\xi - \mu k_1^4\Phi_1^2.$$

From Eqs. (26) and (27) we have

$$\frac{1}{2}\frac{\partial}{\partial t}P_1^2 = 2k_{xy}^2 p_0'\xi + K_i k_y \xi - \kappa k_1^2 P_1^2.$$

From Eqs. (25) we have

$$\frac{1}{2}\frac{\partial}{\partial t}|p_0'|^2 = -k_{xy}^2 p_0'\xi - \chi^{\rm nc} k_0'^2 |p_0'|^2.$$

Also from Eqs. (23)–(24) and Eqs. (26)–(27), we have

$$\frac{\partial}{\partial t}\xi = 2k_{xy}^2 p_0'\Phi_1^2 + K_i k_y \Phi_1^2 - \kappa k_1^2\xi + \frac{1}{1+k_1^2}\left[-(1-K_i k_1^2)k_y\zeta + gk_y P_1^2 - \mu k_1^4\xi\right]$$

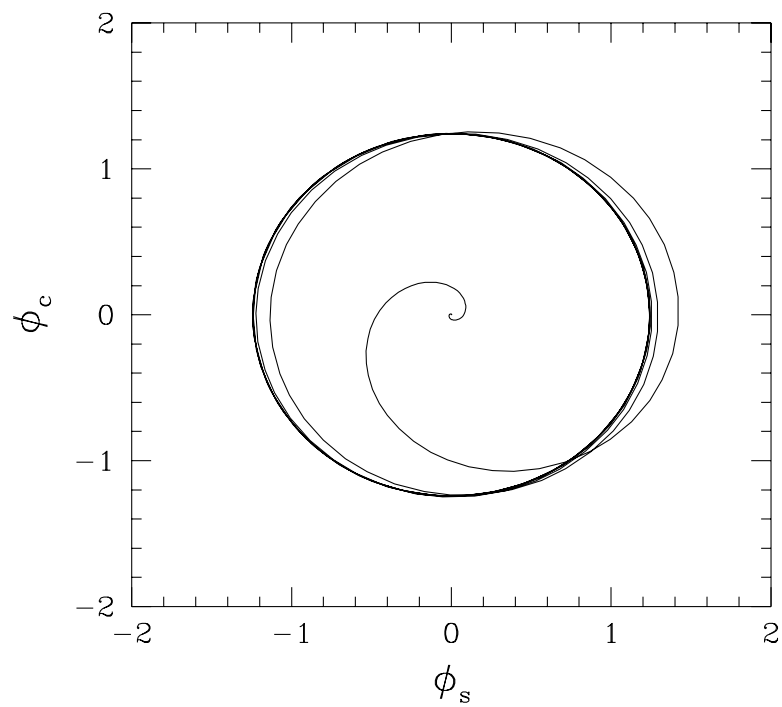

Figure 2: The projection of the phase space trajectory on to the ϕ_c–ϕ_s plane. (a)L-mode limit cycle, (b) L-H transition, (c) L-H-BLM transition.

and

$$\frac{\partial}{\partial t}\zeta = -\kappa k_1^2\zeta + \frac{1}{1+k_1^2}\left[(1-K_i k_1^2)k_y\xi - \mu k_1^4\zeta\right].$$

Then for a stationary state on the limit cycle we have

$$gk_y\xi - \mu k_1^4\Phi_1^2 = 0 \tag{28}$$

$$2k_{xy}^2 p_0'\xi + K_i k_y\xi - \kappa k_1^2 P_1^2 = 0 \tag{29}$$

$$-k_{xy}^2\xi - \chi^{\rm nc} k_0'^2 p_0' = 0 \tag{30}$$

$$2k_{xy}^2 p_0'\Phi_1^2 + K_i k_y\Phi_1^2 - \kappa k_1^2\xi + \frac{1}{1+k_1^2}\left[-(1-K_i k_1^2)k_y\zeta + gk_y P_1^2 - \mu k_1^4\xi\right] = 0 \tag{31}$$

$$-\kappa k_1^2\zeta + \frac{1}{1+k_1^2}\left[(1-K_i k_1^2)k_y\xi - \mu k_1^4\zeta\right] = 0. \tag{32}$$

The solution of this system gives:

$$-A\xi^2 + B\xi = 0, \tag{33}$$

where

$$A = \frac{gk_y\cdot 2k_{xy}^4}{\chi^{\rm nc}k_0'^2}\left[\frac{1}{\mu k_1^4} + \frac{1}{\kappa k_1^2(1+k_1^2)}\right] \tag{34}$$

$$B = K_i g k_y^2\left[\frac{1}{\mu k_1^4} + \frac{1}{\kappa k_1^2(1+k_1^2)}\right] - \frac{(1-K_i k_1^2)^2 k_y^2}{[\mu k_1^4 + \kappa k_1^2(1+k_1^2)](1+k_1^2)}$$
$$- \frac{1}{1+k_1^2}\left[\mu k_1^4 + \kappa k_1^2(1+k_1^2)\right] \tag{35}$$

The thermal flux on the attractor is

$$q_x = \frac{1}{4}k_y\xi = \frac{k_y}{4}\frac{B}{A} = 2K_i\chi^{\rm nc}\left[1 - \frac{u^2(k_1)\mu\kappa k_1^6}{gK_i[\mu k_1^4 + \kappa k_1^2(1+k_1^2)]^2} - \frac{I_c}{I}\right]. \tag{36}$$

For $k_1^2 = 1/K_i$ the ITG-thermal flux reduces to the Rayleigh-Benard convective thermal flux

$$q_x^{r-g} = 2\chi^{\rm nc}\left(K_i - \frac{\mu\kappa k_1^6}{gk_y^2}\right) = \frac{2\chi^{\rm nc}}{g}(I - I_c) \tag{37}$$

which is the same as HHL. The general formula Eq. (36), however, shows that the drift-wave frequency reduces the thermal flux from the value given by the resistive-g dynamics in Eq. (37). On the L-mode attractor the limit cycle frequency is close to the linear mode frequency $\omega_{\mathbf{k}}^{\ell}$ at marginal stability. The amplitude of the limit cycle increases as $(I - I_c)^{1/2}$.

In a torus this convective flux on the L-mode attractor is proportional to the neoclassical thermal diffusivity $\chi^{\rm nc}$. The enhancement of the convective flux over the neoclassical flux in the L-mode is then limited by this low-dimensional model to a factor of approximately two on the L-mode attractor.

B. Second and third bifurcations

As the effective Rayleigh number $\mathrm{Ra}^{\rm eff}$ is increased, the shear flow and the secondary modes are destabilized parametrically by the primary L-mode fluctuations. The bifurcation diagram in the parameter space $(\mathrm{Ra}^{\rm eff}, \mathrm{Pr})$ is given in Fig. 1. Here in principle we can take the values given by the L-mode limit cycle in Eqs. (28)–(35) as known and consider the stability of the L-mode limit cycle to all the other modes in Eqs. (12)–(22), however, the algebra involved is too complicated to warrant writing out. [If the formulas are required the procedure used in HHL can be repeated for this higher dimensional system.] Thus we prefer to present the numerical simulations of the low-order equations (28)–(32). In the simulations we have chosen $K_i = 1.6$, $k_x = 0.3$, $k_y = 1/\sqrt{K_i} \approx 0.8$ to make the first unstable mode in the maximum growth rate region in k-space as discussed in Sec. A.. We also take $\mu = 0.015$ and $\kappa = 0.1$ so the Prandtl number $\mathrm{Pr} = 0.15$.

The L-H transition is clearly seen in the time history plot of the convection flow amplitudes shown in Fig. 3. During the transition, the shear flow increases while the fluctuation amplitudes decrease and they settle down to a new limit cycle on which all the modes are excited, we call this new limit cycle a H-mode attractor. The phase of the primary and secondary modes also rotate on the limit cycle according to a frequency close to the linear

frequency. The projection of the trajectory in the phase space on to the ϕ^s–ϕ^c plane is given in Fig. 2 which clearly show the evolution to the new limit cycle. Similar to Fig. 4 in HHL, the convective flow pattern changes from closed, rectangular cells with no momentum flux $\langle v_x v_y \rangle = 0$ to tilted cells with a net momentum flux $\pi_\perp = \langle v_x v_y \rangle \neq 0$ driving the shear flow $\overline{v}_y = d\phi_0/dx$ against the viscous neoclassical damping. This titling of the cells for the creation of the shear flow is a generic signature in the Rayleigh-Bénard type of fluid models of turbulence [4, 9].

As the effective driving strength Ra is further increased, the H-mode limit cycle is no longer stable against a Hopf bifurcation which forms a new (second) limit cycle of the *modal* amplitudes, the frequency of these oscillations is determined by the critical condition for the Hopf bifurcation and is not related to the linear frequency of the phase rotation of the mode. The shear flow and the flux also show similar oscillations in this state. In the literature, such

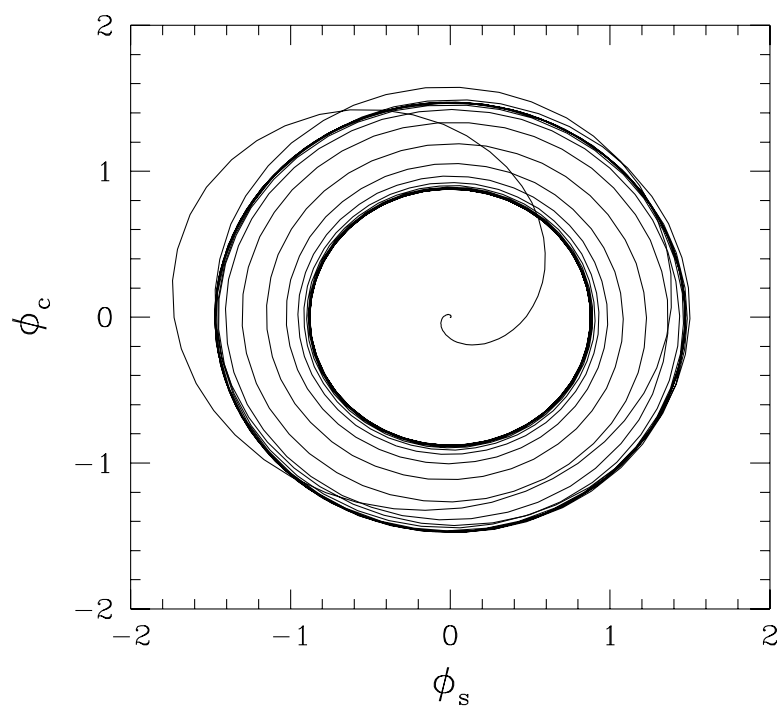

Figure 3: The dynamics of the L to H transition. (a) the $\phi_0(t)$ and $\phi_1(t)$ solutions exponential departure from the neighborhood of the unstable Lorenz manifold and approach to the stable H-mode manifold. (b) the drop in the convective thermal flux.

oscillatory states are usually termed as the ELM (Edge-Localized-Mode) state [14, 15]. Here the ITG turbulence model studied in this work is typically valid only in the core region of the plasmas. In recent higher temperature plasma experiments where the tranport barrier is formed in the core [16], the intermittent breaking of the barrier by oscillatory modes is observed. These interior barrier oscillations are now called a BLM for Barrier-Localized-Mode. The variation of the ELM or BLM frequency $\nu(P_{in})$ with increasing power delivered to the transport layer is an important diagnostic to identify and classify the ELMs and BLMs. In earlier works with resistive-g models the frequency $\nu(P_{in})$ was shown to have first a decrease with P_{in} characteristic of type III ELM and then an increase characteristic of the type ELM. We added the input power term P_{in} in Eq. (18) and this term can be effectively taken into account by the transformation $p_0' \to p_0' + P_{in}/(\kappa k_0^2)$ in Eq. (18) and $K_i \to K_i^{\rm eff} = K_i + P_{in}/(\kappa k_0^2 k_x)$ in Eq. (19) and (20). In Fig. 5, we plot the BLM frequency of

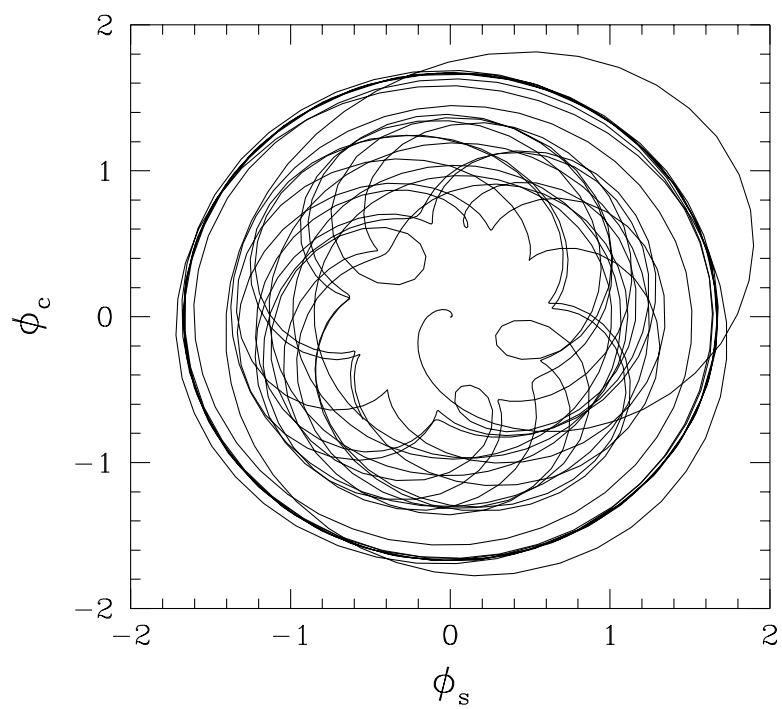

Figure 4: The dynamics of the L to BLM transition. (a) the $\phi_0(t)$ and $\phi_1(t)$ solutions exponential departure from the neighborhood of the unstable Lorenz manifold and approach to the oscillatory BLM-mode manifold. (b) the oscillation in the convective thermal flux.

flux and modal amplitude of the first mode as a function of the driving strength I. The BLM frequency increases with increasing P_{in}, which is similar to the signature of type I ELMs in the edge transport barrier studies. For large P_{in}, faster relaxation oscillations are required to transport the higher input power $P_{in}\sin(2k_x x)$.

The characteristic frequency $\nu(P_{in})$ is given here without attempting to argue that the type I ELM or BLM is an ITG-shear flow recurrence oscillation. The understanding of these complex phenomena is incomplete and the information given may be useful in narrowing the range of applicable models. For example, the discharge in Ref. 17 is a high beta poloidal discharge with $I/aB = 1.4\,\mathrm{MA}/(0.7\ \mathrm{m})(4.4\ \mathrm{T}) \simeq 0.5$ and $q_{\mathrm{eff}} = 6.4$ having both BLM and ELMS. The authors of Ref. 16 state they are performing MHD stability analysis in an attempt to identify the BLM relaxation oscillations at the internal transport barrier.

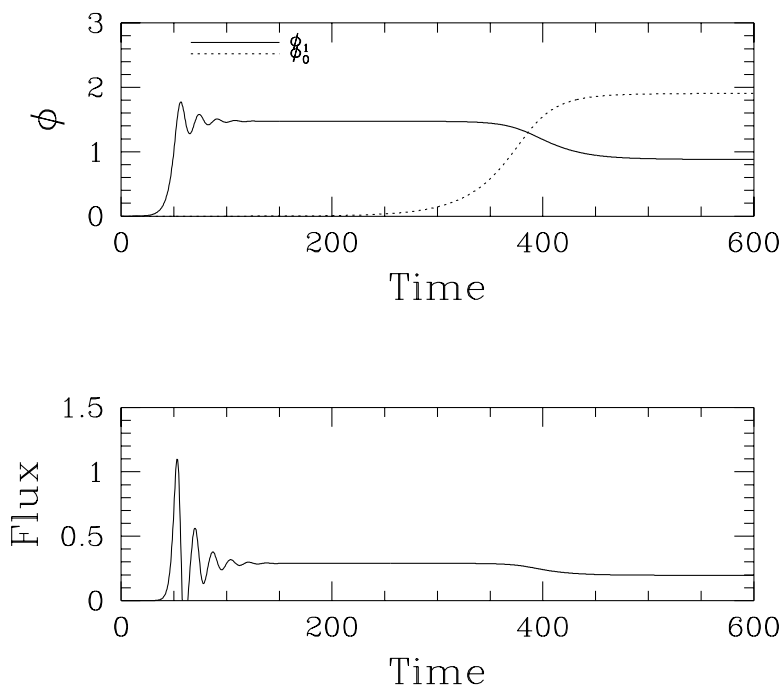

Figure 5: Angular frequencies from the time series of $\phi_0(t)$ and $\phi_1(t)$ as a function of increasing Rayleigh number $(g * K_i)$ past the point of the Hopf bifurcation by the third instability. Adding an external input power parameter P_{in} in the $\dot{p}_0$ equation results in an effective $\mathrm{Ra}^{\mathrm{eff}}$, so this plot can also be interpreted as an equivalent variation of the angular frequency of the BLM-type oscillation versus P_{in}.

C. Pump depletion in the dissipationless limit

When the dissipation terms are omitted from Eq. (12)–(22) the system executes nonlinear amplitude oscillations with a period set by the total energy of the initial state. To test for the inviscid nonlinear behavior we start the system with small amplitude initial conditions in ϕ_1 (with other fields zero), the resulting pulsations are shown in Fig. 6.

The system trajectory is a high dimensional version of the orbit near the separatrix of a pendulum. At small amplitude there is the exponential growth of (ϕ_1, p_1) from the linear growth rate $\gamma^l \approx (gK_i)^{1/2}$. The energy for the fluctuations comes from the background pressure gradient which is reduced by the reaction of (ϕ_1, p_1) by driving up p_0'. The pump depletion process is reversible in that the system overshoots the stable point and returns to its initial amplitude state. When the second mode is also driven unstable and started with small amplitude initial conditions along with the first mode discussed above, the shear flow ϕ_0 is also excited. Then in addition to the pump depletion which reduces the energy source

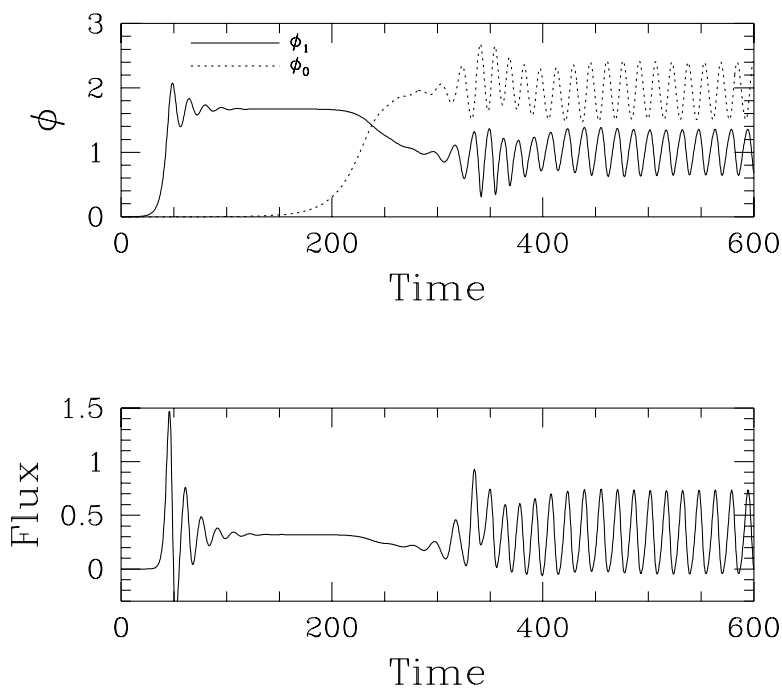

Figure 6: Pump depletions in the dissipationless limit.

and growth rate, the nonlinear frequency shifts indroduced by the shear flows also help stop the growth of the system by taking the system out of the resonance. In this latter case, chaos is often observed which is typical for low-dimensional Hamiltonian systems. An analysis of the nonlinear oscillation in a simpler model of ITG turbulence is given in Horton [17]. We comment here that these pump depletion oscillations in the dissipationless dynamics of the ITG model also contribute to the BLMy oscillations in the full dynamics with dissipations.

D. Higher dimensional representation

The low-order models are useful paradigms for the physics contained in the partial differntial equations but clearly do not resolve the spatial structure. Studies on the truncation errors that occur for the Rayleigh-Benard system are given in Prat *et al.* [18] and Thiffeault and Horton [5]. For the drift wave problem Waltz *et al.* [12] reports on a resolution study showing that 40×10 perpendicular modes are required for convergence. For the chaotic regime of the Rayleigh-Benard problem $(24)^2$ modes are required in the case considered by Prat *et al.* Thus, the low-order truncations must be viewed as a *minimal model* whose solutions exhibit properties that parallel or mimic those of the full system, but give numerical values that can be far removed from those of the full system.

Solutions of the low-order system are useful for interpreting those of the full system. To illustrate this point we show the isopotential contours in a low μ/κ simulation of Eqs. (1) and (2) at the end of the linear phase before a wide spectral range is excited. In Fig. 7 the originally horizontal convective cells with $k_x \ll k_y$ show the tilting due to the shear flow component and the beginning of the splitting of the elongated cells into half their original π/k_x-size from the growth of the $\sin(2k_x\, x)$-Fourier components. The peseudospectral simulation is carried out with a $(128)^2$ FFT for a $(85)^2$ physical grid with $k_1\rho_s = 0.1$. For the parameters $K_i = 3$, $g = 2\epsilon_n = 0.05$, $\mu = 5 \times 10^{-4}$ and $\kappa = 0.015$ the fastest growing mode $\mathbf{k} = (1, 5)k_1$ is in the process of saturating at time shown. Subsequent to the excitation of the

low-order modes contained within the low-order truncation, many other **k**-modes are excited resulting in a turbulent steady state of roughly circular vortices. The final states are characterized by states of large-scale coherent vortices in a sea of turbulent small-scale fluctuations. The energy spectrum $E(k)$ summed over all directions shows $E(k > k_0) = E_0(k_0/k)^{3+\epsilon}$ with $\epsilon \simeq 0.5$ spectral index for $k_0 \simeq 0.7 < k < k_d = 2$. This example makes clear both the usefulness and the limits of the low-dimensional model.

There is a procedure based on extensive post-processing of well-sampled fields, either from simulations or diagnostic sensors, for constructing the principal low-order nonlinear modes of a system by the proper orthogonal decomposition of the two-space point correlation matrix. The eigenfunctions and positive-definite eigenvalues of the correlation matrix sort the field into basis functions of decreasing importance in terms of a mean square error. The projection and truncation of the full system on these numerically generated basis functions, called the

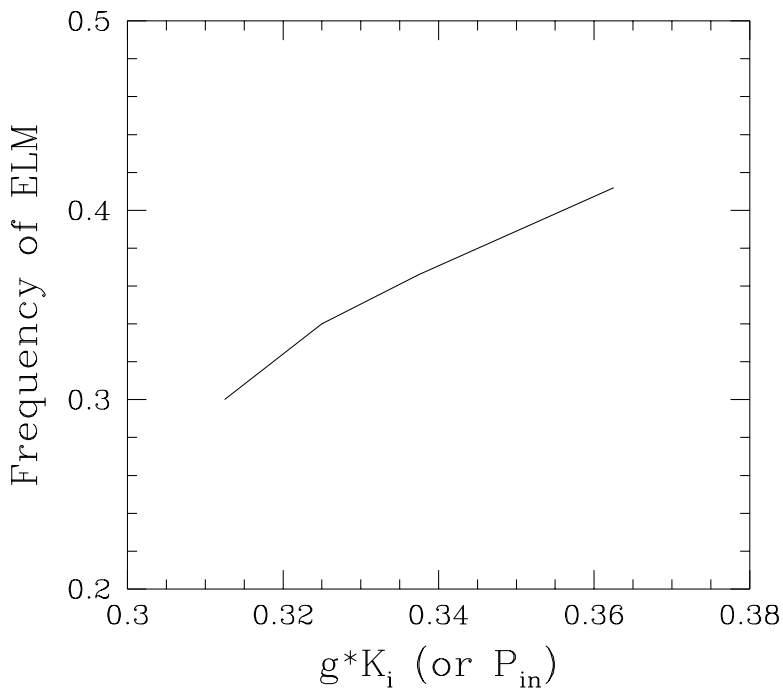

Figure 7: The isopotential contours during the nonlinear saturation of high resolution **k**-space simulation discussed in Sec. III.D.

Karhunen-Loeve expansion, has been carried out by Eickermann and Spatschek [19] for the dissipative drift waves in a weakly ionized plasma. The procedure is computationally intensive and the convergence of the transition must be checked. In Ref. 19 the convergence is reported as very good (with respect to the original 64×128 grid simulation used to generate the correlation matrix) for a projection keeping the first twenty Karhunen-Loeve eigenfunctions.

IV Markovian Closure Models

In close analogy to the resistive-g model of HHL, we investigate the flow of energy through the physically distinct energy components consisting of the effective potential energy $U(t)$, the turbulent kinetic energy $W(t)$ and the kinetic energy $F(t)$ in the mean flows. The three components are defined by

$$U = \frac{g}{K_i}\,(|p_0|^2 + |p_0'|^2),$$

$$W = \tfrac{1}{2}\,[(1+k_1^2)(|\phi_1^s|^2 + |\phi_1^c|^2) + (1+k_2^2)(|\phi_2^s|^2 + |\phi_2^c|^2) - \frac{g}{K_i}(|p_1^s|^2 + |p_1^c|^2) - \frac{g}{K_i}(|p_2^s|^2 + |p_2^c|^2)]$$

$$F = k_x^2 \phi_0^2.$$

where U arises from the change in the local average gradient (quasilinear flattening), W from the sum of kinetic and potential energy in the fluctuations (with W positive-definite for stable profiles $gK_i < 0$) and F from the kinetic energy in the mean (sheared) flow $\overline{\mathbf{V}} = v_y(x,t)\widehat{\mathbf{e}}_y$.

In Fig. 8 the evolution of the three energy components shear flow F, fluctuation energy W, and potential energy U is shown. The thermodynamical variables F, W, U change rapidly during the L-H transition, which is expected. The total energy $(F + W - U)$ suffers a much smaller change during the transition in this 11-D model. The dominant fractional change is the drop in the fluctuation energy W and the increase of the shear flow energy F.

The equations for the $\dot{U}$, $\dot{W}$ and $\dot{F}$ can be easily calculated from Eqs. (12) to (22) and

involve the following triplet correlation functions

$$T_F = \langle (\phi_1^c \phi_2^s - \phi_1^s \phi_2^c)\phi_0 \rangle, \tag{38}$$

$$T_U = \langle (p_1^s \phi_2^c - p_1^c \phi_2^s + p_2^s \phi_1^c - p_2^c \phi_1^s) p_0 \rangle + 2\langle (p_1^c \phi_1^s - p_1^s \phi_1^c) p_0' \rangle. \tag{39}$$

Here the ensemble average $\langle \cdots \rangle$ may be defined over a set of initial conditions (ϕ_i, p_i).

Calculating the rate of change of U, W, F from Eqs. (12) to (22) and adding in external sources P_U and P_F of energy and momentum, we obtain

$$\frac{dU}{dt} = \frac{g}{K_i} k_{xy}^2 T_U - \epsilon_U + P_U, \tag{40}$$

$$\frac{dW}{dt} = -k_{xy}^2 (k_2^2 - k_1^2) T_F + \frac{g}{K_i} k_{xy}^2 T_U - \epsilon_W, \tag{41}$$

$$\frac{dF}{dt} = k_{xy}^2 (k_2^2 - k_1^2) T_F - \epsilon_F + P_F, \tag{42}$$

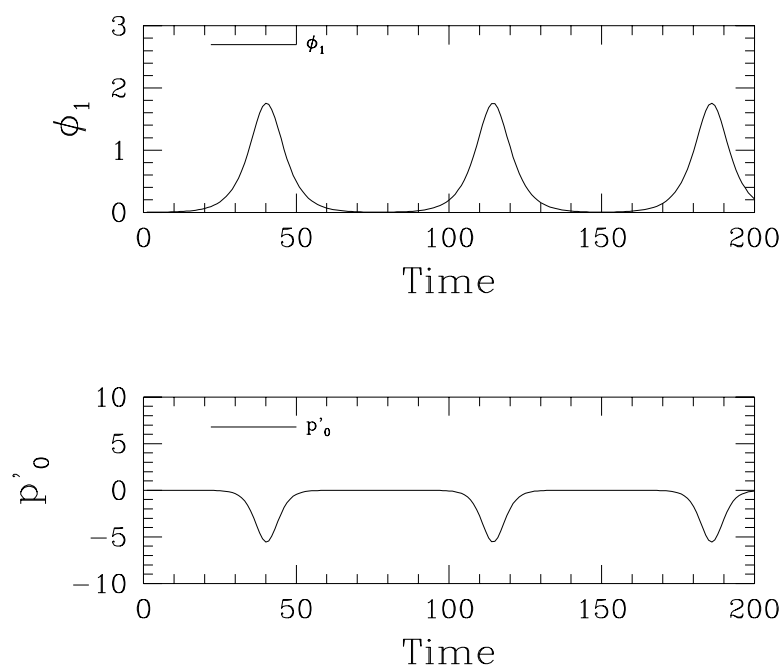

Figure 8: The evolution of thermodynamical variables F, W, U during the L to H transition.

where the dissipation rates are given by

$$\epsilon_U = \frac{g}{K_i}\,\kappa(k_0^2 p_0^2 + {k_0'}^2 {p_0'}^2),$$

$$\epsilon_W = \mu[k_1^4(|\phi_1^s|^2 + |\phi_1^c|^2) + k_2^4(|\phi_2^s|^2 + |\phi_2^c|^2] - \frac{g}{K_i}\,\kappa[k_1^2(|p_1^s|^2 + |p_1^c|^2) + k_2^2(|p_2^s|^2 + |p_2^c|^2)] \quad (43)$$

$$\epsilon_F = k_0^2(\nu_L + k_x^2\mu)\phi_0^2. \quad (44)$$

The ensemble averaged equations follow from Eqs. (40)–(42) with the triplet correlation functions defined in Eqs. (38)–(39) give the average power transfers between U and W and F.

Here we assume that the second harmonic mode ϕ_2, p_2 is linearly stable (damped as $e^{-\nu_2 t}$) and has a low energy content compared to the fundamental mode ϕ_1, p_1. We calculate ϕ_2, p_2 as driven by ϕ_0, ϕ_1, p_0' and introduce a Markovian (local in time) expansion in the time history integrals. The result gives the closure formula for the kinetic energy transfer rate

$$T_F = \left\langle \frac{\partial v_y}{\partial x}\,\pi_{xy} \right\rangle = (\tau_{\rm c}/\Delta^2)W(t)F(t)$$

where $\tau_{\rm c}$ is the nonlinear effective triplet interaction time and Δ is the effective width of the shear flow layer. The structure of this formula for T_F is the same as studied extensively for three-wave interactions [20] where the problem is to determine the nonlinear $\tau_{\rm c}$ for ensemble averaged three-wave interactions.

The driven response of the damped harmonic mode is given by

$$(\frac{\partial}{\partial t} + L_2)X_2 = k_{xy}^2(\phi_0 Y_1 + p_0 Y_1'), \quad (45)$$

where the second harmonic mode

$$X_2(t) = \begin{pmatrix} \phi_2^s(t) \\ \phi_2^c(t) \\ p_2^s(t) \\ p_2^c(t) \end{pmatrix} \quad (46)$$

and the fundamental mode

$$Y_1(t) = \begin{pmatrix} -\dfrac{k_0^2 - k_1^2}{1+k_2^2}\ \phi_1^c(t) \\ \\ \dfrac{k_0^2 - k_1^2}{1+k_2^2}\ \phi_1^s(t) \\ \\ p_1^c \\ \\ -p_1^s(t) \end{pmatrix}, \qquad Y_1'(t) = \begin{pmatrix} 0 \\ \\ 0 \\ \\ -\phi_1^c(t) \\ \\ \phi_1^s \end{pmatrix} \tag{47}$$

are connected by the linear matrix L_2

$$\begin{pmatrix} \mu\frac{k_2^4}{1+k_2^2} & -\frac{(1-K_i k_2^2)k_y}{1+k_2^2} & 0 & \frac{gk_y}{1+k_2^2} \\ \\ \frac{(1-K_i k_2^2)k_y}{1+k_2^2} & \mu\frac{k_2^4}{1+k_2^2} & -\frac{gk_y}{1+k_2^2} & 0 \\ \\ 0 & -K_i k_y & \kappa k_2^2 & 0 \\ \\ K_i k_y & 0 & 0 & \kappa k_2^2 \end{pmatrix}. \tag{48}$$

The closure proceeds by eliminating the second harmonic mode X_2 in terms of p_0 and ϕ_0 and the fundamental mode Y_1 and Y_1'. The exact solution of Eq. (45) with the initial condition $X_2(t_0 \to -\infty) = 0$ is

$$X_2(t) = k_{xy}^2 \int_0^\infty d\tau\, e^{-\tau L_2}[\phi_0(t-\tau)Y_1(t-\tau) + p_0(t-\tau)Y_1'(t-\tau)] \tag{49}$$

where the matrix propagator is $\exp(-\tau L_2) = \sum_n (-\tau L_2)^n/n!$. Eq. (49) is an exact, non-Markovian expression for X_2 and the resulting triplet corrletation involves the nontrival time integrals. Our goal here is to find a small expansion parameter ϵ_M than can be used to Markovianize the expression in Eq. (49).

To be consistent with the numerical simulations presented so far, we have assumed the secondary mode is heavily damped, i.e. the roots of $\det(\gamma I + L_2) = 0$ have $\mathrm{Re}(\gamma) < 0$. Further we assume the leased damped mode γ_+ still decays faster than the time rate of change of $\phi_0 Y_1$ and $p_0 Y_1'$ then the system enters the Markovian domain where the triplet correlation

functions depend only on the local values of the fluctuations. For sufficiently fast damping γ_+ compared with $\gamma_E = |\partial_t \ell n(\phi_0 Y_1)|$ we can expect the expansion $Y_1(t-\tau) = \sum_n (-\tau)^n Y_1^{(n)}(t)/n!$ to converge. The successive terms contribute $\int_0^\infty d\tau \tau^n \, e^{-\tau L_2} = n! L_2^{-n-1}$ to the Markovian expansion of Eq. (34). The first N-terms give

$$X_2 = k_{xy}^2 L_2^{-1}[\phi_0(t)Y_1(t) + p_0(t)Y_1'(t)] - k_{xy}^2 L_2^{-2}\partial_t[\phi_0(t)Y_1(t) + p_0(t)Y_1'(t)] + \cdots$$

$$+k_{xy}^2(-1)^N L_2^{-N-1}\partial_t^N[\phi_0(t)Y_1(t) + p_0(t)Y_1'(t)]. \tag{50}$$

The expansion parameter ϵ_M can then be defined as

$$\epsilon_M = ||L_2^{-1}|| \max_t |\partial_t \ell n[\phi_0(t)Y_1(t) + p_0(t)Y_1'(t)]| \, .$$

In the small expansion parameter limit, i.e. $\epsilon_M \ll 1$, we have the Markovian approximation for the soution of X_2

$$X_2 = k_{xy}^2 L_2^{-1}[\phi_0(t)Y_1(t) + p_0(t)Y_1'(t)] \tag{51}$$

which then can be substituted in the expressions for the triplet correlation functions for the closure of the turbulent transfers in terms of the energy variables F, W and U. Here we use the quantum mechanics matrix notation [9] $\langle 1,2,3,4|L|Y_1\rangle$ and find the kinetic energy transfer function

$$T_F = \phi_0\phi_1^c[\phi_0\Big\langle 1|L_2^{-1}|Y_1(t)\Big\rangle + p_0\Big\langle 1|L_2^{-1}|Y_1'(t)\Big\rangle]$$

$$-\phi_0\phi_1^s[\phi_0\Big\langle 2|L_2^{-1}|Y_1(t)\Big\rangle + p_0\Big\langle 2|L_2^{-1}|Y_1'(t)\Big\rangle]. \tag{52}$$

In Eq. (52) the formulas for inverting the 4×4 matrix L_2 are very complicated; for simplicity we can approximate $(1 - K_i k_2^2) \approx 0$ in the L_2 and get the inverse L_2^{-1} for this particular value of k_2^2. The approximation is good since k_x^2 is much smaller than k_y^2. After tedious algebric manipulations, we find that the terms involving p_0 cancelled out and the final form for T_F in terms of the first harmonic mode and shear flow mode is:

$$T_F = \tau F(t) K_1(t)(\kappa + \frac{\mu k_1^4}{k_2^2(k_1^2 - k_0^2)}) \tag{53}$$

where the coefficient τ is

$$\tau = \frac{2k_2^2}{k_0^2(1+k_1^2)(\mu\kappa k_2^6/k_y^2 - gK_i)},$$

and $K_1(t) = \frac{1}{2}(1+k_1^2)\Phi_1^2$ is the kinetic part of the energy W. In obtaining Eq. (53) the relation between the thermal flux and the Φ_1^2 of Eq. (29) is used.

Eq. (53) can be reduced further using the linear relationship between ϕ_1 and p_1 and the resulting closure formula for the kinetic energy transfer function has the form

$$T_F = \tau_f F(t) W(t) \tag{54}$$

where the coefficient τ_f depends only on the parameters $\{g, K_i, \mu, \kappa, k_x, k_y\}$ in the original dynamical equations.

Similar procedure can be followed to find the closure formula for T_U

$$T_U = \tau_u U^{1/2}(t) W(t) \tag{55}$$

where τ_u is the closure coefficient analogous to τ_f in Eq. (59) to be derived in the same manner.

V Discussion and Conclusions

In this work we extend the study of the low-order mode coupling model of the resistive-g turbulence to the toroidal ion-temperature-gradient model of HCT, which in turn is an application of the well-known low-order mode coupling model [4] of the Rayleigh-Bénard system. The major difference between resistive-g and toroidal ITG model is that the coupled vorticity and pressure equations Eq. (1) and (2) of the two-component toroidal ITG model involve the FLR-drift-waves. The stability analysis shows that the dispersive linear phase rotation plays a more important stabilizing role than the $\mu\kappa$-dissipation term that is the sole stabilizing term in the traditional Rayleigh-Bénard systems. As a consequence, a new definition of effective Rayleigh number $\mathrm{Ra}^{\mathrm{eff}}$ is introduced. The important feature is that

$\mathrm{Ra}^{\mathrm{eff}}$ turns out to be independent of the box size, and this is a major deviation of the ITG model from the resistive-g model and the classical Rayleigh-Benard system.

The minimal low-order coupling model of the toroidal ITG system consists of 11-ODE mode coupling equations that include necessarily the linear drift waves. Three confinement regimes defined in Fig. 1 have been identified in the bifurcations of this 11-ODE reduced system, the L-mode, H-mode and the BLM states. The L-mode attractor (a fixed point in the resistive-g model) evolves to a limit cycle on a 5-d sub-maniford of the phase space with the linear phase rotations. While at first appearance it would seem that the L-mode limit cycle would require numerical evaluation due to its high dimensionality, we are able to find analytic formulas for the L-mode limit cycle and the associated thermal flux. The H-mode attractor bifurcates from the L-mode limit cycle when the shear mass flow is parametrically destabilized by the fluctuation amplitudes and the flux decreases in the dynamical transition. Both the L-mode and the H-mode have steady convection patterns. As the Rayleigh number is increased, the H-mode becomes Hopf unstable and a new convection state with oscillating shear flow and flux forms. These oscillations are similar to the barrier localized modes (BLM) observed in the tokamak confinement experiments. The bifurcation diagram in Fig. 1 summarizes the typical onset conditions of these three regimes.

In Sec. IV, we also investigate the Markovian closure models following the resistive-g study of HHL. The Markovian procedure starts from expressing the driven stable mode in terms of the primary unstable mode. Then we assume that the stable mode is heavily damped so that a Markovian expansion parameter can be defined and in the small limit of this parameter the Markovian approximation procedure can be justified. The resulting Markovian closure model gives a dynamical description of the system in terms of three thermodynamical energy variables: the potential energy from the pressure gradient, the kinetic energy in the sheared mass flows and the turbulent fluctuation energy. The advantage of the Markovian procedure derived here is that the coupling coefficient can be specified in the closure model

whereas in the usual thermodynamical models the coefficients have a great arbitrariness.

Finally, we note that due to the low number of floating point operations required to advance the models developed here, an important application may be to use the model as a real time prediction filter. In this case the coefficients of system may be trained on databases subject to the conservation laws derived here. The main obstacle to this application is the absence of coordinated databases of the relevant input and output signals.

Acknowledgments

This work was supported in part by an appointment to the U.S. Department of Energy Fusion Energy Postdoctoral Research Program administered by the Oak Ridge Institute for Science and Education and in part by the U.S. Department of Energy contract No. DE-AC02-76-CHO-3073.

Appendix A: Model Limitations from Kinetic Processes

Here we discuss two important kinetic effects in more detail. In Eq. (2) the dissipationless threshold for onset of convection from the ion temperature gradient $\eta_i = \partial_x \ell n\, T_i / \partial \ell n\, n = L_N/L_{Ti}$ is given by parameter $K_i = (T_i/T_e)(1+\eta_i - \Gamma) > 0$ where Γ is the effective adiabatic gas constant. For collisionless Vlasov theory the value of Γ is approximately 2 for the toroidal ITG mode as shown in Fig. 2 of Ref. (Kim and Horton, 1991). For the shear slab ITG-mode the ion dynamics is effectively one dimensional so that $\Gamma(1D) = 3$ and $\eta_i^{\rm crit} = 2$. For sufficiently small $k_\perp^2 \kappa$ and $k_\perp^2 \mu$ the damping is finally determined by the fluctuating parallel thermal flux $\widetilde{q}_\parallel$ and the parallel ion momentum flux $\widetilde{v}_\parallel$. These fluxes can be calculated in the linear limit with Landau resonance $\pi\delta(\omega - k_\parallel v_\parallel)$. The effect is to add low-k damping rates proportional to $\kappa_0 |k_\parallel| v_i \cong \kappa_0 v_i/qR$ and $\mu_0 |k_\parallel| v_i = \mu_0 v_i/qR$ to Eqs. (1) and (2). The dissipative operators in Eqs. (1) and (2) should be generalized to have a minimum value given by $\kappa(k) = \kappa_0 + k_\perp^2 \kappa_\perp$ and $\mu(k) = \mu_0 + k_\perp^2 \mu_\perp$ where in the drift wave units we estimate $\kappa_0 \sim \mu_0 \sim \varepsilon_n/q \lesssim 0.05$. This low-$k_\perp$ damping is necessary to achieve a steady state for inverse cascade that fills the box-size modes in the large k-space simulations. Finally we note that Vlasov-Poisson wave frequency $\omega_{\mathbf{k}}^v$ is well known to be given by

$$\omega_{\mathbf{k}} = k_y v_{de} \left[\frac{I_0 e^{-b} + \eta_i b (I_1 - I_0) e^{-b}}{1 + T_e/T_i (1 - I_0 e^{-b})} \right]$$

which for small $b = k_\perp^2 \rho_s^2 (T_i/T_e)$ reduces to

$$\omega_k = k_y v_d \left(\frac{1 - K_i k_\perp^2}{1 + k_\perp^2} \right).$$

Showing the important change of direction of rotation for $k_\perp^2 \simeq 1/K_i$, the growth rates are known to peak near this critical wavenumber from the FULL kinetic Rewoldt code [8]. The coupling to the ion acoustic waves determines the ballooning structure and the formula for k_x but is not important for the mode coupling for fast growing modes [6].

References

[1] E.N. Lorenz, J. Atmos. Sci. **20**, 130 (1963).

[2] L.C. Kells and S.A. Orszag, Phys. Rev. A **162** (1978).

[3] P.W. Terry and W. Horton, Phys. Fluids **26**, 106 (1983).

[4] L.N. Howard and R. Krishnamurti, J. Fluid Mech. **170**, 385 (1986).

[5] Jean-Luc Thiffeault and W. Horton Phys. Plasmas **8**(7), 1715 (1996).

[6] W. Horton, D.-I. Choi, and W. Tang, Phys. Fluids **24**, 1077 (1981).

[7] B.G. Hong and W. Horton, Phys. Fluids B **2**, 978 (1990).

[8] G. Rewoldt and W.M. Tang, Phys. Fluids B **2**, 318 (1990).

[9] W. Horton, G. Hu, and G. Laval, Phys. Plasmas **3**, 2912 (1996).

[10] J-Y. Kim and W. Horton, Phys. Fluids B **3**, 1167 (1991).

[11] J-Y. Kim, Y. Kishomoto, W. Horton, and T. Tajima, Phys. Plasmas **1**, 927 (1994).

[12] R.E. Waltz, G.D. Kerbel, J. Milovich, and G.W. Hammett, Phys. Plasmas **2**, 2408 (1995).

[13] M.A. Beer and G.W. Hammett, Phys. Plasmas **3**, 4046 (1996).

[14] H. Zohm, W. Suttrop, K. Büchl, H.J. de Blank, O. Gruber, A. Kallenbach, V. Mertens, F. Ryter, M. Schittenhelm, ASDEX Upgrade Team, and ICRH-, NBI-Group, Plasma Phys. Control. Fusion **37**, 437–446 (1995).

[15] H. Zohm, Plasma Phys. Contr. Fusion **38**, 1213 (1996).

[16] Y. Koide, T. Takizuka, S. Takeji, S. Ishida, M. Kickuchi, Y. Yamada, T. Ozeki, Y. Neyatani, H. Shirai, M. Mori, and S. Tsajin-Iio, Plasma Phys. Control. Fusion **38**, 1011–1022 (1996).

[17] W. Horton, Plasma Physics **23**, 1107 (1981).

[18] J. Prat, J.M. Massaguer, and I. Mercader, Phys. Fluids **7**, 121 (1995).

[19] Th. Eckermann and K.H. Spatschek, Phys. Plasmas **3**, 2869 (1996).

[20] J.A. Krommes, Phys. Fluids **25**, 1393 (1982).